The Astronomical Journal, 131:2967–2979, 2006 June

PRECISION KINEMATICS AND RELATED PARAMETERS OF THE α PERSEI OPEN CLUSTER

Valeri V. Makarov
Michelson Science Center, California Institute of Technology, 770 South Wilson Avenue,
MS 100-22, Pasadena, CA 91125; vvm@caltech.edu
Received 2005 December 21; accepted 2006 February 21

ABSTRACT

A kinematical study of the nearby open cluster α Persei is presented based on the astrometric proper motions and positions in the Tycho-2 catalog and Second USNO CCD Astrographic Catalog (UCAC2). Using the astrometric data and photometry from the Tycho-2 and ground-based catalogs, 139 probable members of the cluster are selected, 18 of them new. By the classical convergent point method, systematic motions of stars inside the cluster and velocity dispersions are estimated. As directly observed, the upper limit on the internal velocity dispersion per coordinate is 1.1 km s^{-1}. The actual velocity dispersion is much smaller than that value, since all of it appears to come from the expected errors of the astrometric proper motions. The relative position of the convergent point with respect to the cluster stars yields the "astrometric" radial velocity, which turns out larger by a few km s^{-1} than the mean observed spectroscopic radial velocity. This implies an overall contraction of the cluster. Kinematic parallaxes are computed for each member, and an improved H-R diagram is constructed. An age of 52 Myr is determined by isochrone fitting. The star α Per itself fits an isochrone of this age computed with overshooting from the boundary of the convective zone. The theoretical mass of the star α Per is 6.65 $M_\odot$. With respect to the common center of mass, half of the higher mass members (earlier than G) are located within a radius of 10.3 pc. The cluster appears to be roughly twice as large, or as sparse, as the Pleiades, retaining nonetheless a similar dynamical coherence. The low rate of binaries is another feature of this cluster, where we find only about 20% of members to be known or suspected spectroscopic, astrometric, or visual binaries or multiple systems. X-ray emitters in the cluster appear to have the same dispersion of internal velocities as the rest of the membership. The cluster is surrounded by an extended, sparse halo of comoving dwarfs, which are found by combining the proper-motion data from UCAC2 with Two Micron All-Sky Survey infrared photometry. Since many of these external stars are outside the tidal radius, the cluster being in an active stage of disintegration or evaporation could be considered. This hypothesis is not supported by the weak compression and the nonmeasurable velocity dispersion found in the kinematic analysis. A search for stars ejected from the α Persei cluster is carried out by tracking a large number of nearby stars 70 Myr back in time and matching their positions with the past location of the cluster. Only one plausible ejection is found prior to 10 Myr ago. The nearby star GJ 82, an active M dwarf with a strong Hα emission, is likely a former member ejected 47 Myr ago at 5 km s^{-1}.

Key words: binaries: general — open clusters and associations: general — stars: kinematics

Online material: machine-readable table

1. INTRODUCTION

Little is known about the internal kinematics of stars in young, gravitationally bound open clusters. If these clusters are normally formed in very compact and dense molecular clouds, as was proposed by Kroupa (1995), the initial expansion removes very quickly a good fraction of the stars and most of the gas, and the relaxation time is short. In a matter of a few megayears, or sooner, the kinetic energy should be equipartitioned, and more massive stars and binaries should sink closer to the center of gravity. A mass segregation is indeed found in the Pleiades (age $\sim$100 Myr; Raboud & Mermilliod 1998) and in NGC 2547 (Littlefair et al. 2003), but in the latter case only for stars down to 3 $M_\odot$. Smaller mass stars do seem to have a larger velocity dispersion in the Hyades (Gunn et al. 1988; Perryman et al. 1997; Makarov et al. 2000), but the actual reason may be other than the kinetic energy equipartition, for instance, the influence of orbital motions in astrometric binaries. Generally, the estimated velocity dispersions inside the Hyades and the Pleiades are roughly in agreement with theoretical expectations for a dynamically steady and uniform cluster. This has not yet been shown unequivocally for younger and more distant clusters, such as α Persei (age $\sim$50 Myr), mostly due to the paucity of accurate proper motions and radial velocities, but also because of difficulties with membership determination.

Alpha Persei is unusual in some respects when compared with the Pleiades and the Hyades. Being somewhat more distant and considerably younger, this cluster possesses a number of features that differentiate it from the older, better studied counterparts. The most obvious feature is its large size and low number density (Artyukhina 1972), especially of stars more massive than the Sun. The only star evolved off the main sequence is α Per, for which we determine a mass of 6.65 $M_\odot$ in § 5. At the same time, fairly massive probable members of the cluster can be found at 20 pc and farther out (Eddington 1910; Artyukhina 1972). It appears that the cluster is engulfed by a spacious moving group, or "halo" (Shatsova 1981), which has very similar kinematics and photometric properties and was probably formed along with it. What can hold this dispersed group of stars with physical dimensions of roughly 60 pc together for 50 Myr? A large invisible mass of $\approx 10^4$ $M_\odot$ could gravitationally bind stars in a volume that large, since the tidal radius of a cluster along the line toward the Galactic center, in parsecs, is $R_{\rm tid} = 1.4 M_c^{1/3}$, where M_c is the total mass in $M_\odot$ (Adams et al. 2001). A direct observable consequence of a large mass hidden in the cluster is a larger internal velocity dispersion of order 1 km s^{-1} that is proportional to

$M_c^{1/2}$. Furthermore, the stars closer to the central attractor will have larger velocity dispersions than the stars farther out, which is the reverse of the expected internal kinematics of a cluster in a state of energy equipartition. As becomes clear from what follows, precision kinematics analysis puts sufficiently tight upper brackets on these observable parameters to reject this hypothesis.

I examine whether the coordinates of the convergent point of the cluster, as determined geometrically from Tycho-2 proper motions only, are in agreement with the mean distance and radial velocity known in the literature. This allows us to detect possible internal systematic radial motions, such as contraction or expansion. Second, we estimate internal velocity dispersions for various subsets of the cluster in an attempt to find out its dynamical state.

Proper motions and positions of stars from the Tycho-2 catalog (Høg et al. 2000a) are the basic astrometric data used in this paper. The catalog, which is believed to include most of the stars brighter than $V_T = 11.5$ mag (except for components of visual binaries and high-amplitude variables), contains hundreds of nearby open cluster members. Magnitudes in the two passbands B_T and V_T are useful when deciding on possible new members of clusters if more accurate ground-based data are not available. The errors of V_T magnitudes are within 0.05 mag at $V_T = 10$ mag and within 0.16 mag at 11.5 mag. The median standard error of proper motions is 2.5 mas yr^{-1} at $V_T = 11.5$ mag and 1.5 mas yr^{-1} at 9.5 mag. Compared to the proper motions in the *Hipparcos* catalog, Tycho-2 has two important assets: it contains more stars, and, based on a 100 yr series of source catalogs, the proper motions are less perturbed by the orbital motions of binary components. The latter advantage was clearly seen in the comparative analysis of the Hyades cluster (Makarov et al. 2000).

The proper motions in Tycho-2 were computed by combining the Tycho-2 positions at the epoch of about 1991.5 with those from the Astrographic Catalogue at the epoch of about 1905 and 143 other transit circle and photographic catalogs, generally at intermediate epochs. Including these extra catalogs gave a stronger determination of proper motions, a higher confidence of identification, and a deeper investigation of individual star's errors. Computing the Tycho-2 proper motions is described in detail in Høg et al. (2000b).

The recently suggested kinematic segregation of X-ray members of the Hyades and Pleiades (Makarov 2000; Makarov & Robichon 2001), i.e., the fact that stars more luminous in X-rays seem to have smaller velocity dispersions, poses new problems for the commonly accepted model of a coeval cluster in a state of dynamical equilibrium. A plausible explanation of the segregation is that the X-ray-active stars are relatively younger and therefore have not reached dynamical equilibrium through interaction with other members. An alternative explanation is that X-ray emission is greatly enhanced in close binaries, which are more massive than single stars and therefore move slower. In this case the X-ray-emitting stars should huddle closer to the center of gravity because of segregation by mass, which has not been observed. Alpha Persei is a younger cluster, and it may be convenient to test the kinematic segregation hypothesis. Unfortunately, its relative remoteness and the lack of measurable physical velocity dispersion leave the negative result found in § 8 inconclusive.

2. DETERMINING THE CONVERGENT POINT

To determine the convergent point of a cluster, we employ a geometric method based entirely on the astrometric proper motions of carefully selected member stars. The parallel motions of stars in space are reflected in the projected tangential motions that cross at one point on the sky, when extended along their great circles. Astrometric errors of the proper motions and the internal dispersion of the velocities of the stars make this crossing point fuzzy, with individual intersections in pairs scattered around the true convergent point. A statistical method should be employed, minimizing a certain function of the proper motions and their errors. Since the sample includes proper motions of various astrometric precision, a vector of relative deviations $(\Delta_i/\sigma_{\Delta_i})$, $i = 1, \ldots, N$, is considered, where Δ_i is the angular difference between the proper-motion direction (in terms of position angle) and the direction from the ith star to the assumed convergent point and N is the number of stars in the sample. The total standard error of Δ is a quadratic sum of the relative proper-motion error in the component perpendicular to the convergent point direction and the relative velocity dispersion in one component:

$$\sigma_\Delta^2 = \frac{\sigma_{\mu\perp}^2}{\mu^2} + \frac{\sigma_v^2}{v^2 \sin^2\lambda}, \quad (1)$$

where λ is the arc between the star and the convergent point. More mathematical detail on this application of the classical convergent point method can be found in Makarov et al. (2000).

A point is sought that minimizes a given norm of the vector. A 2-norm, $\sum_i |\Delta_i/\sigma_{\Delta_i}|^2$, represents the χ^2 value; thus, minimizing the 2-norm is equivalent to a χ^2 fitting. A 1-norm solution, $\sum_i |\Delta_i/\sigma_{\Delta_i}| = \min$, can be useful in cases of imprecise observation or unreliable membership, for it is more robust in the presence of statistical deviants and blunders. I chose the χ^2 fitting, considering the selection of members to be reliable enough, and because of the practical advantage of having error estimates readily from the least-squares formalism.

The algorithm of minimization in use is the simplex downhill method (Press et al. 1992). The method was found to be reliable for valley-like minima, which are normally the case with the problem in question, but it requires three starting points of estimation. There is therefore a certain risk of falling into a local minimum instead of the global minimum. Pairs of very bright stars with large weights (i.e., with relatively small errors of proper motions) can generate separated local minima. Using a lower norm than 2 or introducing a nonzero dispersion σ_v in the model in equation (1) makes the estimator function smoother and eliminates the local minima. Any particular case requires a careful study of the estimator function in the vicinity of the convergent point for the presence of local minima.

Relative weights assigned to the sample stars may be an important issue. The second term in equation (1) can be neglected if the relative contribution of the physical dispersion is small due to a very low σ_v or due to poor astrometric precision (large $\sigma_{\mu\perp}^2$). The convergent point estimation becomes a straightforward procedure. The resulting χ^2 value indicates whether this assumption is valid, in which case it should be close to 1. If it is significantly greater than 1, a nonzero velocity dispersion must be introduced in the model. The estimation becomes iterative; inasmuch as σ_v is needed to compute the convergent point, and vice versa, coordinates of the convergent point are needed to determine σ_v. Moreover, a full iteration also includes the centroid velocity v, which also involves available trigonometric parallaxes or radial velocities. Generally, including the σ_v term in equation (1) makes the weights at different magnitudes more flat and thus decreases the relative weight of the brightest stars. This may change the estimated convergent point position in cases of kinematic segregation inside the cluster.

3. SELECTING MEMBERS OF THE α PERSEI CLUSTER

The comprehensive work by Prosser (1992) on the α Persei cluster provided the framework for my selection of members. The difficulties of discerning real members of this cluster arise from the spatial proximity to the younger dispersed moving groups in Perseus and Taurus and the alignment of its kinematics with the bulk motion of the so-called local association (Eggen 1983; Montes et al. 2001), which includes dispersed stellar populations from 5 to several hundred megayears of age. The cluster is probably embedded in a more spacious and sparse Cas-Tau group that, according to de Zeeuw et al. (1999), has a close convergent point of proper motions and similar distances. Perhaps a completely clear membership list is not achievable, and some contamination from field stars and the Cas-Tau stream should be tolerated. Our aim in constructing the sample is not completeness but reliability. Therefore, all stars marked with "N" (nonmember) and "N?" (possible nonmember) in Prosser's lists are excluded. The only exceptions are made for HE 507, 863, 875, 958, 1102, and 1164, which appear to be probable members. At the same time, quite a few candidates on Prosser's lists indicated as probable or certain members are now discarded, since their proper motions are in disagreement with the common convergent point or are simply too low in magnitude. The stars with lower proper-motion magnitudes but similar directions may be members of the background Per OB2 association.

Three *Hipparcos* stars, HIP 16047 = HE 703, HIP 15327 = HE 357, and HIP 15556 = HE 450, not listed by Prosser (1992) but confirmed by Robichon et al. (1999, hereafter RAMT), are also included. The membership of HE 450 is still doubtful, for it deviates by -2.76 in Δ/σ_Δ. I also include the star α Per itself (HE 605), which is missing in Tycho-2 due to its brightness.

This original selection of members from Prosser's (1992) lists and *Hipparcos* comprised some 110 stars. It became evident in the course of the subsequent work that more members could be found in the Tycho-2 catalog by kinematic and photometric criteria. The final estimation of the convergent point (see § 4) with the 139 bona fide members produced international celestial reference system (ICRS) coordinates $(\alpha,\ \delta) = (96\overset{\circ}{.}9,\ -24\overset{\circ}{.}3)$. Of the original 110 stars, only 6 had Δ larger than 6° in absolute value, that is, 5% of the sample. Without introducing a significant bias, we considered furthermore all Tycho-2 stars with proper motions deviating by not more than 6° from the convergent point, confined to a circle of radius 4° centered on $(\ell,\ b) = (147\overset{\circ}{.}5,\ -6\overset{\circ}{.}5)$. The total number of these stars is 396. The distribution of their proper-motion magnitudes is depicted in Figure 1. The cluster shows up as the powerful peak between approximately 28 and 41 mas yr^{-1}. Extrapolation of the background distribution yields an estimation of the number of interlopers of less than 20 within that interval. There is also a prominent wing extending toward higher proper motions than 41 mas yr^{-1}. It probably includes outlying members that are closer to the Sun than the bulk of the cluster. This geometric convergent point method of preselection is more reliable than the classical proper-motion vector point diagram (e.g., Prosser 1992) because it properly takes into account the projection effects due to the considerable spread of the cluster on the sky.

Using the kinematic parallaxes as described in § 4, a "dirty" H-R diagram was constructed from the observed magnitudes V_T and B_T for stars with proper motions in the range 28–58 mas yr^{-1}. A clearly defined main sequence of the cluster was found, with increasing width toward fainter magnitudes. This increasing spread was in part attributed to the rapidly deteriorating precision of Tycho-2 photometry at faint magnitudes. At this stage the selection was based on astrometric data only (positions and proper motions). No radial velocity or photometric data had been used. The diagram showed that the vast majority of the kinematically selected 174 Tycho-2 stars were true members of the cluster. Only some 30 stars were suspected, photometrically, to be interlopers and were subsequently discarded by using more accurate B and V magnitudes from the literature. Inspecting the diagram also confirmed that the cluster could be kinematically separated from the field stars.

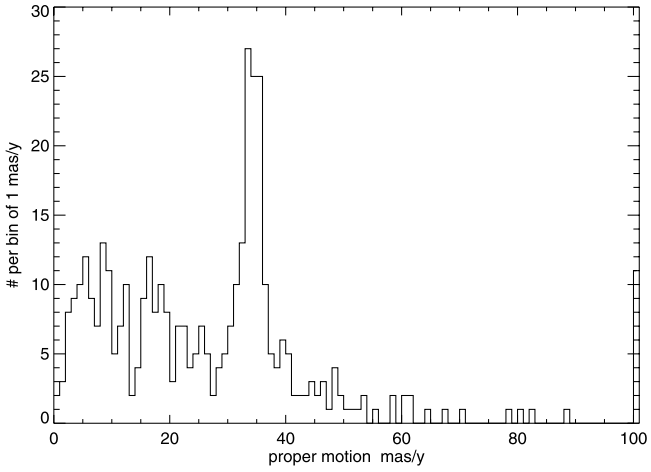

FIG. 1.—Distribution of proper-motion magnitudes of all Tycho-2 stars within 4° of the α Persei center at $(\ell,\ b) = (147\overset{\circ}{.}5,\ -6\overset{\circ}{.}5)$, with proper motions converging in a circle of radius 6° around its convergent point. The presence of the cluster shows up as a strong peak between approximately 28 and 41 mas yr^{-1}, with a tail extending toward higher proper motions.

Finally, the selection is somewhat extended toward larger apparent distances from the center. Assuming a distance of 190.5 pc to the cluster (RAMT), the previous radius of 4° corresponds to 13.3 pc. At the same time, the interval of 28–58 mas yr^{-1}, with the mean at 31 mas yr^{-1}, corresponds to a distance of up to 90 pc on the near side. To somewhat correct this artifact in my selection, I consider all Tycho-2 stars in the annulus of 4°–7° radius with proper motions meeting the same requirements on convergence and magnitudes. An H-R diagram for this sample showed that the interloper rate could reach about 50%. Therefore, only those stars are accepted from the annulus whose membership could be confirmed by radial velocity measures in SIMBAD or in the *Hipparcos* data from de Zeeuw et al. (1999), that is, mostly bright stars.

The resulting sample of α Persei members in Tycho-2 has 139 stars, listed in Table 1. Their positions on the sky in equatorial coordinates are depicted in Figure 2.

4. KINEMATICS AND ROTATION OF α PERSEI

Figure 2 shows the location of the 139 selected stars in equatorial coordinates and the determined position of the convergent point. The coordinates of the convergent point in the ICRS are $(96\overset{\circ}{.}9,\ -24\overset{\circ}{.}3)$ with standard errors $(3\overset{\circ}{.}7,\ 6\overset{\circ}{.}4)$. The 1 σ error ellipse of the convergent point position, as depicted in the inset of the plot, is strongly elongated, reflecting a large correlation of -0.9977. The maximum dimension of the 1 σ error ellipse along the great circle connecting the geometric center of the cluster with the convergent point is $6\overset{\circ}{.}5$. This convergent point determination is in agreement with that in RAMT, $(100\overset{\circ}{.}9,\ -29\overset{\circ}{.}9)$. RAMT also give a CORAVEL-based radial velocity of -0.2 ± 0.5 km s^{-1}. Their convergent point is consistent with the

TABLE 1

HIGH-FIDELITY MEMBERS OF α PERSEI

ID No. (1)	Tycho-2 No. (2)	HE No. (3)	R.A. (4)	Decl. (5)	μ (6)	V (7)	$B-V$ (8)	$V_{\rm abs}$ (9)	V_r Astr. (10)	d (11)	$L_{\rm X}$ (12)	$L_{\rm X}$ Error (13)	Binarity (14)
1.....	3305-0435-1		+02 52 39.9	+48 48 59.8	(24.7, −25.5) ± (1.4, 1.5)	7.04	0.01	0.85	1.31	172			
2.....	3305-0301-1		+02 57 54.1	+48 52 43.6	(23.2, −21.4) ± (1.6, 1.6)	8.71	0.25	2.27	1.61	194			
3.....	3318-1062-1	12	+03 07 50.4	+49 06 30.0	(26.9, −23.6) ± (1.9, 1.9)	10.09	0.51	3.93	2.11	171			
4.....	3318-1509-1		+03 08 14.5	+49 50 22.3	(23.5, −21.7) ± (3.3, 3.0)	11.58	0.68	5.17	1.87	191			
5.....	3310-2437-1		+03 09 24.2	+45 22 59.2	(24.1, −23.1) ± (0.9, 1.0)	8.06	0.11	1.77	3.55	182			
6.....	3314-0559-1	56	+03 09 52.1	+48 28 15.6	(23.6, −22.3) ± (1.9, 1.8)	10.84	0.81	4.47	2.46	188			
7.....	3315-1159-1	94	+03 11 16.8	+48 10 37.0	(27.4, −28.0) ± (1.9, 1.8)	10.42	0.64	4.46	2.65	156	23.8	2.0	
8.....	3315-1185-1	104	+03 11 41.1	+48 03 15.1	(31.0, −31.1) ± (1.4, 1.4)	8.60	0.34	2.89	2.72	139			
9.....	3323-1142-1	145	+03 11 42.9	+52 09 48.7	(24.8, −25.1) ± (1.1, 1.2)	6.88	0.03	0.69	1.22	173			
10.....	3319-0519-1	135	+03 11 50.0	+50 22 47.0	(24.0, −23.4) ± (1.6, 1.6)	9.69	0.48	3.39	1.88	182			
11.....	3315-1279-1	151	+03 12 42.6	+47 50 19.2	(23.4, −25.3) ± (1.3, 1.3)	8.97	0.32	2.73	2.86	177			
12.....	3319-0544-1	167	+03 13 05.2	+49 00 34.1	(25.3, −25.6) ± (1.7, 1.8)	7.96	0.11	1.82	2.45	169			
13.....	3319-0446-1	174	+03 13 07.4	+49 34 03.6	(24.1, −30.2) ± (4.2, 3.8)	11.53	0.75	5.54	2.25	158			
14.....	3319-1112-1	212	+03 13 50.3	+49 34 08.2	(26.1, −25.3) ± (1.2, 1.3)	7.16	0.03	1.04	2.29	168			SB
15.....	3319-0771-1	270	+03 15 23.5	+49 26 25.3	(22.7, −21.6) ± (1.6, 1.6)	10.04	0.52	3.60	2.42	194			
16.....	3323-0091-1	295	+03 15 48.7	+50 57 21.5	(33.2, −35.2) ± (1.6, 1.7)	6.71	0.09	1.20	1.88	126			V
17.....	3319-0009-1	299	+03 15 58.9	+50 24 18.9	(19.0, −17.5) ± (2.2, 2.0)	11.12	0.64	4.25	2.10	236			
18.....	3319-1078-1	309	+03 16 23.1	+49 37 33.6	(24.2, −21.8) ± (1.9, 1.9)	9.96	0.49	3.60	2.41	187			
19.....	3323-0323-1	333	+03 16 49.1	+51 13 05.7	(24.1, −23.9) ± (1.4, 1.5)	7.19	0.03	0.92	1.84	180			
20.....	3319-1280-1	334	+03 16 59.4	+49 55 36.0	(22.9, −21.8) ± (2.0, 2.0)	10.37	0.55	3.94	2.33	193			
21.....	3319-1287-1	338	+03 17 20.3	+49 30 07.7	(24.1, −26.1) ± (1.9, 1.9)	9.92	0.53	3.75	2.51	172			
22.....	3319-0306-1	350	+03 17 36.9	+48 50 08.7	(17.7, −19.6) ± (2.3, 2.2)	11.01	0.68	4.19	2.77	231	12.0	3.3	V
23.....	3319-0005-1	357	+03 17 43.2	+50 21 39.9	(31.2, −32.3) ± (1.6, 1.7)	7.51	0.12	1.84	2.21	136			
24.....	3319-0835-1	361	+03 18 01.7	+49 38 39.0	(21.0, −23.0) ± (1.9, 1.9)	9.68	0.43	3.22	2.49	196			
25.....	3319-1383-1	365	+03 18 05.2	+49 54 22.1	(24.0, −24.0) ± (1.6, 1.6)	9.98	0.45	3.71	2.40	180			
26.....	3319-0183-1	379	+03 18 23.9	+50 33 20.8	(26.8, −26.9) ± (1.3, 1.5)	8.06	0.18	2.03	2.17	161			
27.....	3315-1080-1	373	+03 18 27.4	+47 21 15.6	(17.6, −26.9) ± (3.0, 2.7)	11.55	0.80	5.17	3.37	189			
28.....	3319-2073-1	383	+03 18 37.7	+50 13 20.0	(22.7, −26.7) ± (1.0, 1.1)	5.16	−0.07	−1.04	2.31	174			
29.....	3319-0729-1	386	+03 18 44.7	+49 46 12.0	(21.5, −25.8) ± (1.8, 1.8)	7.95	0.11	1.66	2.48	181			
30.....	3319-0589-1	389	+03 18 50.3	+49 43 52.3	(20.1, −28.7) ± (2.2, 2.1)	11.17	0.67	4.97	2.50	174			
31.....	3319-2074-1	401	+03 19 07.6	+50 05 42.1	(21.9, −26.3) ± (1.2, 1.2)	5.04	−0.07	−1.21	2.38	178	<4.7		
32.....	3319-1876-1	421	+03 19 41.7	+48 54 49.3	(22.7, −27.1) ± (1.2, 1.3)	9.23	0.45	3.05	2.86	172	10.8	2.0	
33.....	3315-1908-1	423	+03 19 47.2	+48 37 40.7	(23.6, −24.4) ± (1.9, 2.0)	7.64	0.07	1.37	2.97	179	<2.1		SB1
34.....	3323-0880-1	441?	+03 20 06.2	+50 58 07.8	(23.0, −26.4) ± (0.9, 1.1)	7.06	0.05	0.85	2.11	174			
35.....	3323-1498-1	450	+03 20 23.6	+51 37 06.3	(27.1, −26.5) ± (0.9, 1.0)	7.29	0.01	1.26	1.88	161			
36.....	3315-1781-1	453	+03 20 39.3	+47 29 22.1	(22.5, −18.8) ± (1.8, 1.7)	10.39	0.62	3.81	3.44	207	10.7	2.6	
37.....	3703-0665-1		+03 20 39.6	+52 43 35.7	(28.1, −38.2) ± (2.6, 2.5)	10.78	0.77	5.23	1.47	129			
38.....	3315-1766-1	481	+03 21 30.2	+48 29 38.1	(23.2, −24.1) ± (1.2, 1.2)	9.16	0.39	2.86	3.11	182	<0.8		
39.....	3319-1402-1	490	+03 21 40.2	+49 07 13.0	(24.0, −26.6) ± (1.3, 1.4)	9.56	0.45	3.41	2.89	170	0.7	0.1	
40.....	3319-1538-1	501	+03 21 58.6	+49 12 53.7	(23.5, −25.7) ± (1.3, 1.3)	9.14	0.35	2.93	2.87	175	<0.9		
41.....	3315-1837-1	507	+03 22 03.5	+47 56 04.9	(19.3, −23.3) ± (1.4, 1.4)	8.35	0.12	1.83	3.36	201			SB
42.....	3319-1956-1	520	+03 22 21.9	+49 08 27.8	(21.9, −25.0) ± (2.5, 2.3)	11.67	0.79	5.36	2.92	183	22.7	1.3	SB
43.....	3323-1089-1	522	+03 22 26.3	+51 39 39.7	(19.6, −20.1) ± (1.3, 1.4)	9.13	0.27	2.44	1.97	217			V?, SB?
44.....	3320-2812-1	557	+03 23 13.2	+49 12 48.0	(20.6, −26.5) ± (1.3, 1.4)	5.26	−0.08	−1.03	2.94	181	<0.9		
45.....	3316-0656-1	577	+03 23 40.3	+47 57 29.9	(24.9, −28.4) ± (1.8, 1.8)	9.79	0.68	3.76	3.44	161	2.0	0.6	
46.....	3324-1089-1	575	+03 23 43.1	+51 46 13.5	(23.2, −23.9) ± (1.4, 1.5)	7.88	0.07	1.56	1.99	183			
47.....	3316-1016-1	581	+03 23 47.3	+48 36 16.1	(23.2, −27.0) ± (1.5, 1.5)	6.99	0.01	0.83	3.20	171	22.4	1.3	V
48.....	3320-2190-1	588	+03 23 55.1	+50 18 24.2	(23.1, −26.1) ± (1.6, 1.6)	9.99	0.52	3.78	2.56	175	6.7	0.7	
49.....	3312-2311-1		+03 24 06.5	+46 17 18.6	(25.4, −23.9) ± (1.1, 1.1)	8.72	0.29	2.52	4.09	174			
50.....	3320-2808-1	605	+03 24 19.3	+49 51 40.5	(24.1, −26.0) ± (0.5, 0.6)	1.82	0.47	−4.36	2.75	172			
51.....	3320-0549-1	606	+03 24 19.2	+49 13 16.8	(21.0, −24.8) ± (1.5, 1.5)	8.98	0.33	2.62	2.99	187	1.6	0.5	
52.....	3320-0998-1	609	+03 24 25.0	+50 19 34.9	(22.5, −27.5) ± (1.4, 1.4)	9.23	0.42	3.06	2.58	171	11.9	0.6	
53.....	3320-1499-1	612	+03 24 30.0	+49 08 23.9	(22.9, −25.6) ± (1.9, 2.0)	7.87	0.09	1.63	3.03	177	<1.2		
54.....	3316-0300-1	621	+03 24 47.1	+48 24 42.2	(22.0, −26.3) ± (1.5, 1.5)	9.86	0.49	3.62	3.33	177	<1.0		
55.....	3320-1283-1	622	+03 24 49.7	+48 52 18.6	(23.2, −27.2) ± (3.0, 2.8)	11.66	0.82	5.51	3.15	170	27.6	1.3	
56.....	3316-1050-1	625	+03 24 52.1	+47 54 54.7	(23.7, −26.0) ± (1.6, 1.7)	7.63	0.11	1.44	3.52	173	<1.1		
57.....	3316-1671-1	632	+03 24 55.1	+47 24 54.2	(22.1, −25.9) ± (1.4, 1.4)	9.71	0.48	3.45	3.71	178	<4.7		
58.....	3320-2058-1	635	+03 25 04.3	+49 47 43.7	(22.0, −25.7) ± (1.3, 1.4)	9.05	0.34	2.77	2.82	180	<4.4		
59.....	3320-0805-1	639	+03 25 10.0	+49 15 05.8	(22.0, −24.4) ± (1.3, 1.3)	8.15	0.12	1.81	3.03	185	<0.9		
60.....	3320-1449-1	651	+03 25 20.7	+49 18 58.4	(21.5, −25.1) ± (1.3, 1.3)	8.42	0.19	2.10	3.01	184	<1.0		
61.....	3320-1768-1	660	+03 25 37.6	+50 19 18.2	(19.8, −25.6) ± (1.5, 1.5)	10.10	0.56	3.73	2.64	188	1.3	0.1	
62.....	3316-2317-1	665	+03 25 37.6	+47 01 14.5	(22.6, −25.6) ± (1.0, 1.0)	8.64	0.29	2.39	3.90	178			
63.....	3320-2814-1	675	+03 25 57.4	+49 07 15.0	(21.8, −28.2) ± (1.5, 1.5)	6.06	−0.08	−0.10	3.12	171	<0.8		
64.....	3320-1639-1	684	+03 26 04.2	+48 48 07.3	(21.6, −22.7) ± (2.2, 2.2)	10.54	0.56	4.10	3.25	194	17.1	0.7	

TABLE 1—*Continued*

ID No. (1)	Tycho-2 No. (2)	HE No. (3)	R.A. (4)	Decl. (5)	μ (6)	V (7)	$B-V$ (8)	V_{abs} (9)	V_r Astr. (10)	d (11)	L_X (12)	L_X Error (13)	Binarity (14)
65.....	3316-0358-1	692	+03 26 10.8	+48 23 02.8	(24.3, −28.7) ± (1.4, 1.5)	7.49	0.03	1.45	3.41	162	<0.8		
66.....	3320-0545-1	699	+03 26 22.2	+49 25 37.7	(18.4, −19.0) ± (3.0, 2.7)	11.31	0.70	4.50	3.03	230	41.9	1.3	
67.....	3316-0489-1	710	+03 26 32.6	+47 15 59.4	(24.5, −28.6) ± (1.1, 1.2)	8.18	0.18	2.15	3.86	161			
68.....	3324-0302-1	703	+03 26 39.4	+50 50 47.6	(24.9, −27.4) ± (1.2, 1.4)	7.64	0.08	1.56	2.50	165			
69.....	3320-1715-1	715	+03 26 40.7	+48 46 37.0	(20.4, −25.8) ± (1.9, 1.9)	9.72	0.47	3.38	3.29	185	12.7	0.5	SB2?
70.....	3316-1872-1	721	+03 26 39.2	+47 52 56.5	(21.5, −26.0) ± (1.5, 1.5)	9.66	0.51	3.39	3.63	180	<1.2		
71.....	3320-0818-1	709	+03 26 43.9	+49 54 34.6	(18.3, −23.4) ± (2.3, 2.3)	10.92	0.68	4.36	2.86	205	26.6	2.0	
72.....	3320-1319-1	727	+03 26 50.1	+48 47 32.3	(20.0, −23.5) ± (2.2, 2.1)	10.30	0.55	3.83	3.29	197	16.7	0.7	SB?
73.....	3320-1275-1	733	+03 27 03.2	+48 47 13.6	(22.0, −25.4) ± (1.9, 1.9)	9.94	0.50	3.66	3.31	181	8.4	0.5	
74.....	3316-0698-1	735	+03 27 05.1	+48 12 20.0	(23.9, −25.5) ± (1.3, 1.4)	6.83	−0.02	0.63	3.53	174	<0.7		
75.....	3324-0292-1	732	+03 27 14.1	+50 52 44.1	(23.2, −26.0) ± (1.5, 1.5)	10.17	0.55	3.95	2.51	175	3.7	0.2	A, SB2?
76.....	3320-0423-1	750	+03 27 37.8	+48 59 29.0	(15.8, −26.1) ± (2.2, 2.1)	10.54	0.59	4.05	3.26	199	2.1	0.4	
77.....	3316-0942-1	756	+03 27 37.6	+48 16 22.8	(23.4, −27.1) ± (1.6, 1.7)	7.95	0.10	1.80	3.53	170	<0.8		SB?
78.....	3320-2259-1	747	+03 27 39.0	+49 35 59.9	(22.6, −25.3) ± (1.5, 1.5)	6.99	−0.03	0.72	3.03	180			
79.....	3320-2239-1	767	+03 27 55.0	+49 45 37.4	(18.3, −24.7) ± (2.3, 2.2)	10.66	0.61	4.18	2.98	198	<3.3		
80.....	3316-2251-1	775	+03 27 55.8	+47 44 09.6	(23.9, −27.4) ± (1.7, 1.8)	7.26	0.05	1.15	3.76	167	<1.8		SB1
81.....	2873-0685-1		+03 28 02.9	+44 23 24.9	(31.2, −38.8) ± (1.0, 1.1)	8.12	0.44	2.71	5.03	121			
82.....	3320-2815-1	774	+03 28 03.1	+49 03 46.6	(22.9, −26.0) ± (1.3, 1.3)	4.97	−0.09	−1.25	3.25	175	<0.8		SB2
83.....	3320-0686-1	780	+03 28 18.6	+49 57 10.6	(22.5, −24.6) ± (1.7, 1.7)	8.09	0.17	1.78	2.93	183	15.1	2.6	SB, V
84.....	3320-1731-1	799	+03 28 31.5	+48 56 27.6	(22.2, −27.1) ± (1.9, 1.9)	9.66	0.45	3.46	3.33	174	1.0	0.3	V
85.....	3320-0804-1	794	+03 28 34.6	+50 16 00.9	(22.6, −25.7) ± (1.4, 1.4)	10.09	0.54	3.84	2.82	178	<2.0		SB
86.....	3320-0565-1	802	+03 28 38.0	+49 23 15.7	(21.4, −25.0) ± (1.4, 1.4)	8.41	0.17	2.08	3.16	185	<1.7		SB?
87.....	3320-2809-1	810	+03 28 52.3	+49 50 54.4	(21.7, −26.1) ± (1.6, 1.6)	5.58	−0.04	−0.69	3.00	179	<2.1		
88.....	3320-0399-1	817	+03 28 53.6	+49 04 13.4	(24.6, −31.2) ± (1.9, 2.0)	7.46	0.11	1.54	3.30	153	2.3	0.5	SB1
89.....	3316-1336-1	831	+03 29 07.6	+48 18 10.7	(22.5, −26.9) ± (1.5, 1.6)	7.36	0.01	1.17	3.60	173	<0.7		
90.....	3320-2810-1	835	+03 29 22.0	+49 30 32.5	(19.4, −24.3) ± (2.2, 2.1)	4.66	−0.10	−1.80	3.15	196	14.7	1.3	V
91.....	3320-1057-1	841	+03 29 24.9	+48 57 45.3	(24.1, −25.6) ± (2.0, 2.0)	10.28	0.55	4.09	3.37	173	10.8	0.7	
92.....	3316-1440-1	848	+03 29 26.2	+48 12 11.9	(22.6, −28.1) ± (1.9, 1.9)	9.99	0.59	3.86	3.66	168	3.3	0.5	SB
93.....	2873-0106-1		+03 29 32.1	+43 13 50.8	(22.8, −26.3) ± (1.2, 1.2)	8.90	0.34	2.72	5.56	172			
94.....	3320-0761-1	862	+03 29 47.0	+49 09 13.8	(27.5, −33.3) ± (1.5, 1.6)	8.52	0.31	2.78	3.31	141	<0.5		
95.....	3320-1849-1	863	+03 29 46.8	+49 00 34.5	(23.7, −28.0) ± (1.5, 1.5)	9.21	0.52	3.11	3.37	166	17.4	1.3	
96.....	3316-0985-1	876	+03 29 46.9	+47 34 58.4	(18.8, −27.7) ± (1.5, 1.6)	9.55	0.52	3.26	3.92	181	22.2	1.3	
97.....	3320-1259-1	868	+03 29 51.9	+49 12 48.6	(20.2, −27.2) ± (1.2, 1.4)	7.28	0.09	1.01	3.29	180	<0.7		A, SB1?
98.....	3316-1958-1	875	+03 29 50.0	+47 58 36.8	(22.9, −28.8) ± (1.1, 1.4)	7.66	0.10	1.58	3.77	165	8.0	0.7	
99.....	3316-0896-1	885	+03 30 19.3	+48 29 57.8	(21.6, −28.3) ± (1.1, 1.1)	8.79	0.28	2.63	3.59	171	1.6	0.4	
100.....	3316-2306-1	904	+03 30 36.9	+48 06 13.2	(24.1, −23.5) ± (1.5, 1.6)	5.82	−0.04	−0.46	3.76	180	<0.9		
101.....	3316-1157-1	906	+03 30 34.0	+47 37 41.7	(22.8, −24.5) ± (1.3, 1.4)	8.78	0.28	2.49	3.94	181	<1.6		
102.....	3320-2272-1	921	+03 31 14.7	+49 42 22.7	(21.7, −24.7) ± (1.4, 1.4)	8.59	0.20	2.26	3.17	185	<2.4		
103.....	3320-1652-1	931	+03 31 30.2	+49 54 07.7	(21.7, −26.1) ± (1.4, 1.4)	8.75	0.26	2.48	3.11	179	<6.4		
104.....	3320-0583-1	935	+03 31 29.0	+48 59 28.6	(21.4, −26.9) ± (1.5, 1.4)	10.06	0.64	3.82	3.46	177	45.3	2.0	V
105.....	3316-2310-1	955	+03 31 33.1	+47 51 44.9	(22.3, −25.9) ± (1.4, 1.5)	6.75	−0.02	0.51	3.90	177	<1.3		SB1?
106.....	3320-2520-1	944	+03 31 44.5	+49 32 12.7	(21.8, −25.5) ± (1.5, 1.6)	9.62	0.43	3.33	3.27	181	4.4	1.3	
107.....	3316-0136-1	965	+03 31 53.9	+48 44 06.8	(25.2, −29.0) ± (1.4, 1.5)	6.62	−0.03	0.63	3.59	158	2.6	0.6	A, V, SB1?
108.....	3316-0956-1	968	+03 31 54.2	+48 31 38.6	(22.6, −26.9) ± (1.7, 1.7)	10.41	0.57	4.22	3.67	173	16.8	1.3	
109.....	3316-0994-1	970	+03 31 55.8	+48 35 01.9	(25.3, −30.7) ± (1.4, 1.4)	8.19	0.19	2.27	3.65	152	<0.6		
110.....	3320-2166-1	958	+03 31 58.7	+49 52 12.8	(24.0, −25.9) ± (1.3, 1.3)	9.20	0.39	3.02	3.15	172			
111.....	3316-2307-1	985	+03 32 08.6	+48 01 24.7	(23.2, −23.5) ± (1.4, 1.5)	5.46	−0.10	−0.86	3.87	184	<1.0		
112.....	3324-0799-1	972	+03 32 31.9	+51 29 22.7	(21.0, −22.6) ± (1.4, 1.4)	10.24	0.57	3.76	2.55	197			
113.....	3316-0459-1	1056	+03 33 22.2	+47 25 19.6	(21.4, −27.6) ± (1.4, 1.4)	8.25	0.10	2.06	4.17	173	<4.0		
114.....	3321-0466-1	1050	+03 33 54.3	+50 17 48.2	(21.5, −27.8) ± (1.4, 1.4)	9.48	0.40	3.29	3.08	173	<1.2		SB
115.....	3325-0442-1	1045	+03 33 58.9	+50 52 56.3	(18.7, −26.0) ± (2.0, 1.9)	9.94	0.49	3.54	2.86	190			
116.....	3317-0589-1	1082	+03 34 12.9	+48 37 03.1	(22.5, −27.2) ± (1.5, 1.6)	7.34	0.03	1.16	3.75	172	<2.7		A, V?
117.....	3317-1170-1	1084	+03 34 21.6	+48 39 36.1	(22.2, −29.0) ± (1.6, 1.6)	8.83	0.22	2.73	3.74	166	<2.8		
118.....	3317-1172-1	1102	+03 34 43.3	+47 53 12.7	(19.6, −24.9) ± (2.3, 2.2)	11.03	0.60	4.62	4.06	191	15.7	2.0	SB2?
119.....	3325-0239-1	1086	+03 35 05.0	+50 54 45.4	(18.8, −22.3) ± (2.7, 2.5)	11.32	0.67	4.73	2.90	208			
120.....	3321-1655-1	1101	+03 35 08.7	+49 44 39.9	(19.1, −28.5) ± (2.7, 2.5)	11.25	0.69	5.01	3.36	177	37.2	0.5	
121.....	3317-0354-1	1153	+03 35 58.5	+47 05 27.9	(21.3, −24.5) ± (1.2, 1.2)	6.89	−0.02	0.54	4.44	186			
122.....	3317-3033-1	1164	+03 36 29.4	+48 11 33.7	(19.4, −28.9) ± (1.2, 1.2)	4.20	−0.08	−2.01	4.04	174			
123.....	3317-1064-1	1160	+03 36 31.8	+48 39 16.9	(17.6, −27.7) ± (1.9, 1.9)	10.16	0.49	3.83	3.86	185			
124.....	3321-0187-1	1180	+03 36 55.1	+48 49 43.1	(20.8, −27.8) ± (1.9, 1.9)	10.07	0.49	3.86	3.81	174			
125.....	3317-0016-1	1185	+03 36 57.7	+48 44 45.8	(19.2, −29.5) ± (2.6, 2.5)	11.19	0.72	5.01	3.84	173			
126.....	3317-2554-1	1259	+03 38 15.6	+47 34 37.4	(20.3, −27.4) ± (1.3, 1.4)	7.45	0.00	1.21	4.37	177			
127.....	3317-1930-1	1260	+03 38 35.1	+48 35 36.8	(19.4, −28.3) ± (1.6, 1.6)	8.65	0.22	2.42	3.99	176			
128.....	3313-1551-1		+03 38 50.5	+46 36 12.8	(20.6, −25.9) ± (1.7, 1.7)	10.26	0.52	3.95	4.78	182	151.2	3.5	
129.....	3325-0753-1	1234	+03 39 02.9	+51 36 37.4	(21.5, −34.1) ± (2.3, 2.2)	10.81	0.72	4.91	2.82	151			

TABLE 1—*Continued*

ID No. (1)	Tycho-2 No. (2)	HE No. (3)	R.A. (4)	Decl. (5)	μ (6)	V (7)	$B-V$ (8)	V_{abs} (9)	V_r Astr. (10)	d (11)	L_X (12)	L_X Error (13)	Binarity (14)
130.....	3325-0814-1		+03 40 34.5	+52 00 30.4	(19.6, −26.5) ± (1.3, 1.4)	9.11	0.35	2.78	2.73	185			
131.....	3313-2091-1		+03 41 05.7	+45 47 37.9	(16.8, −25.2) ± (1.3, 1.2)	10.31	0.53	3.82	5.22	199			
132.....	3325-0503-1	1349	+03 41 40.9	+51 16 35.8	(23.6, −30.1) ± (1.2, 1.3)	9.47	0.46	3.46	3.08	159			
133.....	3330-0593-1		+03 45 27.5	+47 39 37.5	(21.6, −27.2) ± (1.2, 1.4)	7.16	−0.01	0.97	4.71	174			
134.....	3326-2124-1		+03 45 53.2	+45 36 00.0	(22.6, −28.5) ± (1.2, 1.3)	7.57	0.07	1.48	5.55	165			
135.....	3334-0408-1		+03 45 54.7	+50 25 09.5	(19.2, −26.2) ± (1.2, 1.2)	9.46	0.37	3.10	3.62	187			V?
136.....	3326-1225-1		+03 49 01.0	+46 48 10.0	(21.9, −26.4) ± (1.6, 1.7)	7.91	0.19	1.69	5.23	176			
137.....	3326-3074-1		+03 53 39.5	+45 45 29.5	(20.9, −26.0) ± (1.1, 1.2)	8.59	0.21	2.32	5.89	179			
138.....	3331-2472-1		+04 00 20.5	+47 34 18.3	(17.3, −25.9) ± (1.2, 1.2)	8.37	0.20	1.94	5.47	193			A
139.....	3339-1125-1		+04 01 50.0	+50 38 17.8	(21.2, −29.6) ± (1.4, 1.5)	8.05	0.12	1.95	4.26	166			

NOTES.—Col. (1): ID number. Col. (2): Tycho-2 number. Col. (3): HE number from Heckmann et al. (1956). Cols. (4) and (5): Right ascension and declination (J2000.0). Units of right ascension are hours, minutes, and seconds, and units of declination are degrees, arcminutes, and arcseconds. Col. (6): Proper motion and its errors in mas yr^{-1}. Col. (7): V magnitude. Col. (8): $B-V$ color. Col. (9): Absolute V magnitude. Col. (10): Astrometric radial velocity in km s^{-1}. Col. (11): Kinematical distance in parsecs. Col. (12): X-ray luminosity L_X in 10^{29} ergs s^{-1}. Col. (13): Error of L_X. Col. (14): Binarity flag (V for visual binaries, A for astrometric, and SB for spectroscopic). Table 1 is also available in the electronic edition of the *Astronomical Journal*.

quoted radial velocity and a *Hipparcos*-based distance of 190 pc through the well-known relation

$$v_{\rm rad} = v_{\rm cen} \cos\lambda = \frac{4.74\mu}{\pi} \cot\lambda, \qquad (2)$$

where λ is the angular distance between the star (of the cluster center in this case) and the convergent point, $v_{\rm cen}$ is the modulus of the centroid velocity, μ is the magnitude of the proper motion in mas yr^{-1}, and π is the parallax in mas. The smallness of the observed $v_{\rm rad}$ is due to λ being close to 90°, and it is quite insensitive to error in π.

Our geometrically determined convergent point is several degrees closer to the cluster. A centroid heliocentric velocity $v_{\rm cen}$ of 30 km s^{-1} is adopted, which gives an average distance of 183 pc from the classical equation $v_{\rm cen} \sin\lambda = 4.74\mu/\pi$, in close agreement with the value by Pinsonneault et al. (1998) from main-sequence fitting. The centroid radial velocity, by equation (2), is +3.2 ± 3.3 km s^{-1}. This astrometric radial velocity is weakly dependent on the assumed magnitude of the centroid velocity because the velocity vector is nearly orthogonal to the line of sight, and cos λ in equation (2) is close to 0. Taking into account the gravitational redshift of spectral lines, which is smaller than 1 km s^{-1} for main-sequence stars, makes the difference between the spectroscopic and astrometric radial velocities even larger. Madsen et al. (2003) discuss a possible absolute blueshift of spectral lines in rapidly rotating stars, which may be larger than 3 km s^{-1} for stars earlier than F5. This effect is hardly important in our case, because the CORAVEL-based radial velocities in RAMT are obtained for members later than F5, for which the (hypothetical) convection-driven blueshifts are small. Therefore, the closer position of the convergent point found in this paper may be interpreted as mild contraction of the cluster. However, this result, taken alone, is not statistically significant, because this estimate is just outside 1 σ of the observed value. On the other hand, this result is bolstered by the study by Madsen et al. (2002), who derived an astrometric radial velocity of +4.5 ± 2.2 km s^{-1} from *Hipparcos* data. Therefore, a slight contraction of the cluster cannot be ruled out. Alternatively, both *Hipparcos* and Tycho-2 proper motions may suffer from a common systematic error in this area.

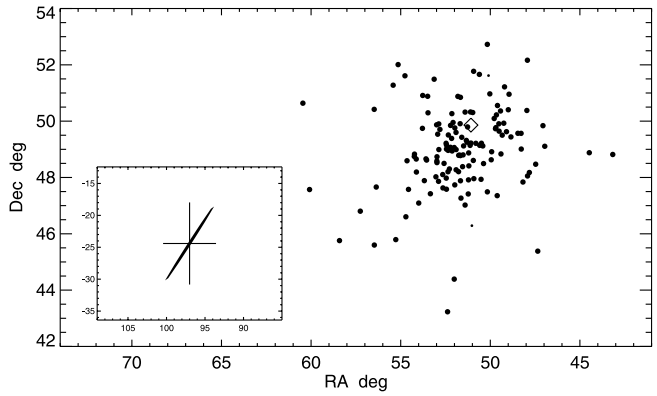

FIG. 2.—Sky positions of α Persei members selected from Tycho-2 in equatorial coordinates (J2000.0). The two stars with $|\Delta/\sigma_\Delta| > 2.5$, possibly nonmembers, are marked with smaller dots. The star α Per is indicated with an open diamond. The inset shows the position of the convergent point (*in the crosshair of the error bars*) determined by a χ^2 fitting from the proper motions, its formal standard errors, and the highly elongated ellipse of covariance. The convergent point is approximately 83°.8 away from the cluster's center.

To further illuminate the issue of systematic contraction or expansion, I determine convergent points for stars within 8.5 pc of the cluster's center and outside this radius. For the former groups of stars a convergent point at $\lambda = 82° \pm 18°$ is found, while for the latter, $\lambda = 82° \pm 8°$. No significant difference is found between the inner core and the outer halo of the cluster. The precision of convergent point determinations in the direction perpendicular to the great circle connecting the center of the cluster and the convergent point is much better than along this great circle. I determine a position angle of the convergent point, reckoned north through east, of 138°.1 ± 0°.3 for the outer halo against 139°.7 ± 0°.3 for the inner core. It is likely that the halo exhibits a small change in the direction of motion due to, perhaps, the effect of Galactic tidal forces. The core stars are further divided into two approximately equal groups of those closer to the convergent point in the celestial projection and those farther out. For the former group, the position angle is 140°.9 ± 0°.3, and for the latter, 139°.6 ± 0°.3. The difference can be understood as a slow (but measurable) counterclockwise rotation of the core in the projection on the sky. A rough estimation of the rotation period yields 230 Myr.

Using the high precision of Tycho-2 proper-motion direction and the equation

$$v_\perp \sin\lambda = \frac{4.74\mu_\perp}{\pi}, \qquad (3)$$

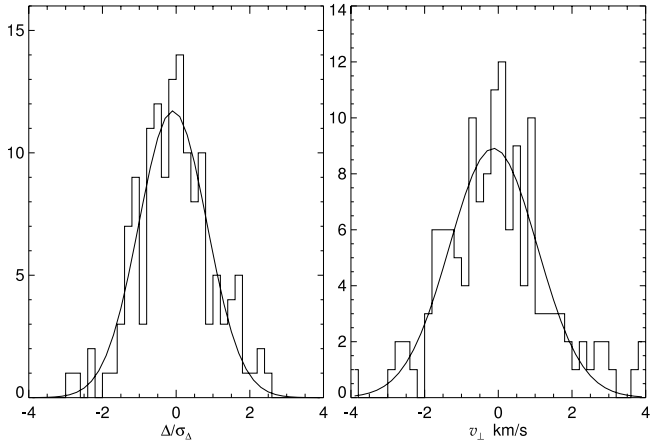

FIG. 3.—Distributions of relative deviations of proper-motion directions from the convergent point direction and of transverse velocities for cluster members from Tycho-2. Gaussian fits are shown, which are used to determine the standard deviations.

the intrinsic one-dimensional velocity dispersion in the tangential component perpendicular to the convergent point direction can be computed, which is an important parameter directly related to the total mass and the actual dynamical state of the cluster. Figure 3 shows the distributions of the weighted residuals Δ/σ_Δ calculated by equation (1) with $\sigma_v^2 = 0$ and of the perpendicular tangential velocities in km s^{-1}. Both distributions are fitted with Gaussians very well, the latter corresponding to $\sigma_{v_\perp} = 1.1$ km s^{-1}. The fit to the residuals corresponds to a standard deviation of less than 1. This could happen if a large number of genuine members with proper-motion directions deviating by more than 1 σ_Δ from the convergent point were rejected, which appears unlikely due to the lax kinematic criteria used in this selection. Therefore, the formal errors of the proper motions in Tycho-2 are probably overestimated, and the actual precision is considerably higher in this area. It could be a local occurrence, because the formal errors are derived from stellar magnitudes, so that zonal changes in the overlapping plate schemes in the Astrographic Catalogue are not captured (S. Urban 2001, private communication). In any case, the width of the weighted residual distribution implies that all of the spread in $v_\perp$ is due to astrometric random errors. These results are consistent with a zero velocity dispersion in the cluster. In the unlikely event that the precision of Tycho-2 is severely underestimated, the physical one-dimensional dispersion may be a fraction of the upper bound (1.1 km s^{-1}).

5. H-R DIAGRAM, AGES, AND MEMBERSHIP

Having determined λ for each star, we can estimate the distance by reversing equation (2). Such "kinematic" distances are substantially more precise than the *Hipparcos* parallax-based distances. The latter are precise to about 20%–30%, while the former are precise to about 6%. Figure 4 shows the H-R diagram constructed on these improved distances for all 139 stars. The *BV* photometry is adopted from Prosser (1992) for all previously known members. For the new suggested members, the Johnson magnitudes are computed from the B_T and V_T magnitudes in the Tycho-2 catalog, applying the photometric calibration relations in Høg et al. (2000b) and the zero-point corrections determined by Maíz-Apellániz (2005). Known binary stars of all kinds are marked with crosses.

It is remarkable that a 52 Myr isochrone computed with a substantial efficiency of overshooting (Pietrinferni et al. 2004)

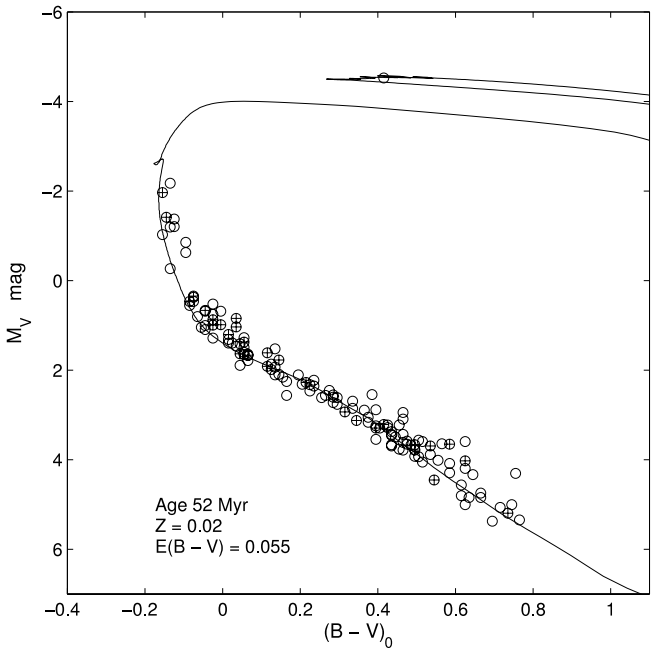

FIG. 4.—H-R diagram of the α Persei cluster. The isochrone of 52 Myr with overshooting computed from the models by Pietrinferni et al. (2004) is shown for comparison. Known binaries of all kinds (spectroscopic, astrometric, and visual) are marked with crosses. The only star brighter than $M_V = -4$ mag is α Per itself.

fits the location of the star α Per, by far the most luminous and massive member of the cluster. The corresponding theoretical mass of the star is 6.65 $M_\odot$. Both the age and the mass estimates are in excellent agreement with the previous isochrone fit by Meynet et al. (1993), whose models also used a moderate degree of convection overshooting. Canonical models (without overshooting) by Pietrinferni et al. (2004) do not match the photometric parameters of α Per. This appears to be evidence in favor of stellar models with overshooting provided by a study, somewhat surprisingly, of a very young cluster. This age is also in agreement with previous estimations from the lower main sequence by Stauffer & Hartmann (1986) and Stauffer et al. (1989) but significantly lower than Prosser's (1992) result.

The remaining scatter around the main sequence in Figure 4 significantly exceeds the standard deviation of 0.13 mag along the M_V axis expected from the remaining uncertainty of individual distances and photometry errors. Some (but not all) of the known spectroscopic binaries are indeed located far above the isochrone, but several apparently single stars are also too bright or too red compared with the rest of the cluster. The binary census of the cluster was studied in depth by, most notably, Morrell & Abt (1992) and Patience et al. (2002). The paucity of spectroscopic binaries in general, and the lack of binaries with periods shorter than 20 days, makes the chances of the deviants from the main sequence to be undiscovered close binaries slim. Furthermore, Morrell & Abt (1992) note the small mass ratios for the few binaries among the more massive members and interpret this fact as an early stage of binary formation by capture. The low dispersion of velocities in the cluster is in agreement with this surmise, because the tightening of binaries through dynamical interaction should be quite slow. I find a few more astrometric and resolved visual binaries (§ 7), but undiscovered binarity can still hardly explain the apparently overluminous members.

Using low-resolution spectra and $E(V-I)$ color excesses, Prosser (1992) investigated the possibility of interstellar differential

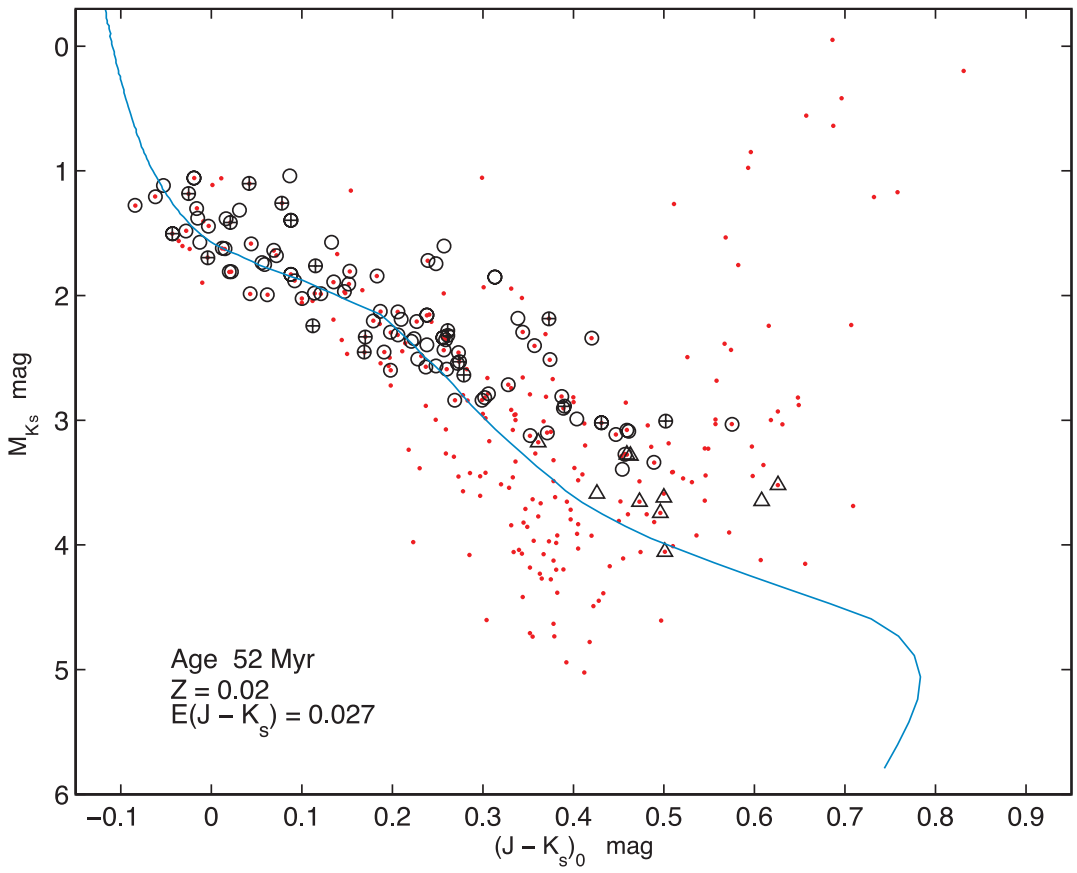

FIG. 5.—H-R diagram of the α Persei cluster in the 2MASS near-IR passbands. The isochrone of 52 Myr with overshooting computed from the models by Pietrinferni et al. (2004) is shown for comparison. Known binaries of all kinds (spectroscopic, astrometric, and visual) are marked with crosses. Red dots represent all stars within 10° of α Per on the sky, with proper motions from UCAC2 converging near the cluster's convergent point and proper-motion components within 10 mas yr^{-1} of the mean cluster's proper motion. Additional possible members (not in the Tycho-2 catalog) identified in the literature are marked with open triangles.

reddening in the cluster. If a small part of the cluster is obscured by a minor cloud within its boundaries, the reddened stars may be confined to a certain region on the sky. No such confinement was found, the reddened stars being randomly dispersed across the map (his Fig. 14). This analysis can be further refined taking into account the distribution of stars in depth. If the hypothetical layer or shred is close to the center, the reddened stars should be more distant than the unreddened ones. For each star in Figure 4, an empirical reddening is determined as the distance to the theoretical main sequence along the line of interstellar extinction. When these color excesses are plotted against the kinematic distances from Table 1, column (11), no correlation is found, indicating that the most "reddened" stars are randomly spread across the range of distances.

Another independent test for the differential reddening assumption comes from a cross-examination of accurate optical and near-IR magnitudes for the probable members. Figure 5 depicts an H-R diagram based on the J, H, and K_s photometry from the Two Micron All Sky Survey (2MASS). Again, in construction of this diagram the more accurate kinematic distances were used instead of the mean parallax for all stars. Probable members of the cluster from Table 1 are marked with open circles, with crosses inside the circles for known binaries. A 52 Myr isochrone with overshooting from the same model by Pietrinferni et al. (2004) as in Figure 4 is given for comparison. The theoretical Johnson K magnitudes were transformed into K_s magnitudes by the Koorneef transformations in Carpenter (2001). The diagram was dereddened according to the relations derived from Bonatto et al. (2004):

$$A_{Ks} = 0.73E(J - K_s), \tag{4}$$

$$E(J - K_s) = 0.488E(B - V). \tag{5}$$

We find again a large spread of probable members (marked with open circles) to the right of and above the main sequence. Some stars with higher masses are also found below the main sequence, but this scatter is in rough agreement with the 6% uncertainty in individual distances from the kinematic method (0.13 mag in absolute magnitude). At the same time, a number of probable members appear to be too luminous or too red on the other side of the main sequence. If differential interstellar extinction is responsible for this asymmetric spread, the same stars should be reddened in the optical and near-IR colors. Empirically derived color excess data for the most outlying stars are shown in Figure 6. The solid line shows the expected interstellar reddening relation. Obviously, the occurrence of color excess in the near-IR is not correlated with that in the optical. By the same argument, another possible explanation for the deviant stars is refuted. If there were a group of stars coincident with the cluster and moving in the same direction as the cluster at a smaller velocity, the kinematic method would overestimate their luminosities, placing them above the main sequence. In this case, too,

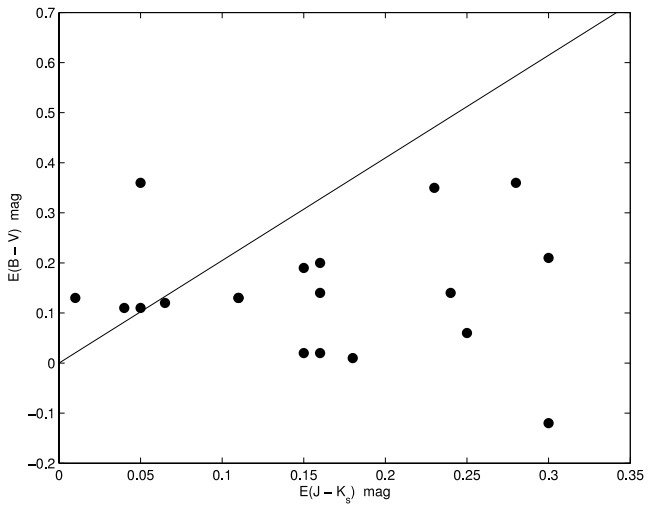

FIG. 6.—Color excess for the most reddened, nonbinary members of α Persei in the optical ($B - V$) and in the near-IR ($J - K_s$).

the same stars would have appeared overluminous in all spectral bands.

6. SECOND USNO CCD ASTROGRAPHIC CATALOG AND 2MASS DATA

Membership lists of low-mass stars can be refined using accurate proper motions from the Second USNO CCD Astrographic Catalog (UCAC2; Zacharias et al. 2004). In this area of the sky, this catalog achieves excellent precision, comparable to that of the Tycho-2 catalog, but it extends to fainter magnitudes and is conveniently cross-referenced with 2MASS. Using this accurate astrometric and near-IR photometric information, I investigate whether more probable members can be found outside the traditionally adopted radius of 4°. First, 748 stars are selected from UCAC2 situated within 10° of the star α Per with proper-motion components in the intervals $\mu_{\alpha \cos \delta} = 25 \pm 10$ and $\mu_\delta = -28 \pm 10$ mas yr^{-1} and with formal errors less than 5 mas yr^{-1} in each coordinate. A more refined kinematic selection is further made by selecting only stars whose extended proper-motion directions (great circles) deviate from the previously determined convergent point at $(\alpha,\ \delta)_{\rm CP} = (96\overset{\circ}{.}9,\ -24\overset{\circ}{.}3)$ by less than 1 σ_Δ. This stringent criterion is intended to reduce the number of false positives outside the projected tidal radius of the cluster. Column (11) in Table 1 shows that a significant number of probable members are situated outside a 10 pc radius along the line of sight. A 10° radius on the sky corresponds to 32 pc at the mean distance to the cluster. Therefore, finding possible members at large angular separations from the cluster's center confirms the existence of a very extended halo that is not gravitationally attached to the main system, but in all evidence was formed simultaneously with it.

Figure 5 depicts with small dots all stars from UCAC2 meeting these simple astrometric criteria. The larger markers show previously identified probable members. Absolute magnitudes M_{K_s} are computed assuming all stars share the same velocity $(U,\ V,\ W) = (-15.0,\ -25.3,\ -7.6)$ km s^{-1}. Background nonmembers, which are more distant than the cluster, fall below the main sequence, while foreground stars lie above and to the right of the main sequence. The graph reveals that a large degree of contamination with nonmembers is expected if one only relies on the proper-motion requirements. This contamination seems to be limited to intermediate- and low-mass stars, because almost all stars with $J - K_s < 0.2$ follow the cluster's main sequence quite closely, and may belong to the cluster. These stars have masses larger than about 1.5 $M_\odot$. Most of those not identified as previously known probable members (Fig. 5, *small dots*) are outside the 3° radius of the core of the cluster. At the mean distance to α Persei, 3° is subtended by 9.7 pc. This is equal to the tidal radius in the direction to the Galactic center if the total mass of stars enclosed is 330 $M_\odot$ (see § 10). In view of the rather low density of genuine members even in the core region, it is doubtful that the tidal radius is significantly larger than 10 pc. Therefore, we find strong evidence that there exist stars in considerable numbers that appear to be related to the cluster but, being far outside the tidal radius, are not gravitationally attached to it.

Nine more fainter members from UCAC2 and 2MASS, confirmed by X-ray data in Randich et al. (1996), and one from Prosser & Randich (1998) are marked with open triangles in Figure 5. These stars are AP 97, AP 102, AP 14, AP 25, HE 696, AP 63, HE 828, HE 917, AP 199, and APX 61 (the AP nomenclature is from Stauffer et al. [1985]). Although their number is insignificant in comparison with the previously discussed Tycho-2 collection, the fainter extension of the near-IR H-R diagram that they provide is welcome because it confirms the curious deviation of the main sequence from the theoretical isochrone at $J - K_s \approx 0.3$ (1.3 $M_\odot$). Members with masses lower than 1.3 $M_\odot$ ($M_{Ks} > 3$) are overluminous in K_s by roughly 0.1 mag, resulting in redder $J - K_s$ colors. A similar discrepancy with theoretical isochrones is seen in the near-IR diagrams for the Pleiades at ≈100 Myr in Bonatto et al. (2004). Older clusters, such as Praesepe and M41, do not seem to have this feature. Stauffer et al. (2003) investigated in depth the color anomalies of K dwarfs in the Pleiades. In this cluster the prominent overluminosity of low-mass stars in the near-IR K_s band is accompanied by an overluminosity of about the same magnitude in the blue optical bands (U and B). Stauffer et al. suggest that this peculiarity of the spectral energy distribution is a manifestation of the high activity and spottedness of these young stars, implying a very large areal filling factor of >50% of cool spots and correspondingly large plage areas. They note that in still younger clusters, e.g., in NGC 2547, color anomalies seem to extend to earlier spectral types, at least to G. One may wonder if the K_s excess we find for F stars in α Persei can be explained along these lines.

7. BINARIES

Known or suspected binary stars are indicated in Table 1. This information was mostly collected from Prosser (1992), Morrell & Abt (1992), and Patience et al. (2002). In addition to their data, I find five new astrometric binaries. The star HIP 16088 = HE 732 has an acceleration solution in *Hipparcos* of $(\dot{\mu}_{\alpha*},\ \dot{\mu}_\delta) = (11.27,\ 7.79) \pm (3.84,\ 3.36)$ mas yr^{-2}, and its *Hipparcos* proper motion of (19.5, −33.4) mas yr^{-1} deviates from the Tycho proper motion of (23.2, −26.0) mas yr^{-1}. The star HIP 16277 = HE 868 also has an acceleration solution, $(\dot{\mu}_{\alpha*},\ \dot{\mu}_\delta) = (5.67,\ -1.01) \pm (2.26,\ 3.17)$ mas yr^{-2}; however, its *Hipparcos* and Tycho-2 proper motions are consistent. Three other astrometric binaries, HIP 16450 = HE 965, HIP 16649 = HE 1082, and HIP 18697, have differences between the *Hipparcos* and Tycho-2 proper motions in excess of 3 σ, but no detected accelerations. This implies, statistically, orbital periods of >6 yr (Makarov & Kaplan 2005). Binaries with detectable accelerations in α Persei have full semimajor axes around 5–6 AU and periods 8–13 yr, quite close to the most frequent separation of 4 AU, according to Patience et al. (2002). It is unusual that there are only two accelerating binaries in our sample.

Three of the visual binaries in Table 1, TYC 3323-91-1 and 3323-91-2 = HIP 15193A and 15193B, HE 350, and

HE 835 = HIP 16244, are resolved into components in the Tycho Double Star Catalog (TDSC; Fabricius et al. 2002) with separations of 1.″46, 0.″89, and 0.″87, respectively. *Hipparcos* was capable of resolving visual binaries down to a 0.″1 separation, which corresponds to ≈18 AU at the average distance of the cluster. No such close binaries were detected by *Hipparcos*, however. Counting all types of binaries, only ≈20% of members are binaries. This is modest even compared with field G dwarfs and much smaller than the binarity rate in the nearest clusters, Hyades and Pleiades. Another peculiarity of α Persei is the paucity of visual binaries with large separations. TDSC lists three wide pairs in the cluster, all of which are optical pairs due to discordant proper motions and photometry: (1) HE 490 is listed as the B component to TYC 3319-2075-1 (WDS 03219+4904); (2) HE 665 is the A component to HIP 15970 (WDS 03256+4701); (3) HE 955 = HIP 16430 has a B component in *Hipparcos* with a "stochastic" solution (WDS 03316+4752).

8. X-RAY STARS

Stars in open clusters are known to have widely ranging X-ray luminosities. Solar-type stars of the same mass, age, and, presumably, chemical composition differ in X-ray brightness by at least 2 orders of magnitude. This type of stellar activity is not, therefore, defined by the above-mentioned fundamental properties. On the other hand, considering only stars detected by the *ROSAT* PSPC instrument, a clear statistical decline of X-ray activity with age has been discovered among nearby open clusters. The mean $\log L_X$ (in ergs s^{-1}) for G stars drops from 29.7 in α Persei to 29.4 in the Pleiades at 80 Myr (Randich et al. 1996), and further to 28.9 at 600 Myr for the Hyades (Stern et al. 1995). There exists, therefore, a relation to age, but not a direct one. Blueward of spectral type G, X-ray emission is usually not detected, with the exception of a few quite bright sources, which are most probably unresolved binaries whose less massive companion is responsible for the anomalous radiation. The X-ray flux at K and M dwarfs gradually tapers off because of the smaller corona surfaces; in terms of $\log L_X/L_{bol}$ the relation becomes flat at $B - V = 0.8$ mag due to the saturation level at about -3 (Stauffer et al. 1994; Prosser et al. 1996). It was suggested that the degree of X-ray activity among G, K, and M dwarfs of the same age is determined mostly by the rate of rotation, which varies widely in open clusters (Stauffer et al. 1994). Generally, the most luminous X-ray sources are also the most quickly rotating stars. However, this relation is not strict, as slowly rotating (according to their low observable $v \sin i$) stars are sometimes powerful emitters approaching the saturation limit. The origin of the spread in X-ray activity in open clusters is not yet understood.

Information about X-ray emission from the literature is collected in Table 1 for roughly half of the Tycho-2 sample. The references are Randich et al. (1996) and Prosser et al. (1996, 1998). Note that the X-ray luminosities in the table are recomputed with the kinematically estimated distances from the convergent point method, which may give significant improvement for stars well separated from the center of mass in the radial direction, e.g., HE 350. For nondetections the upper limits of luminosity are given (e.g., $<0.6 \times 10^{29}$ ergs s^{-1} for HE 970). Positive detections have standard errors of L_X in column (13). Stars missed in the dedicated X-ray surveys and not identified in the general *ROSAT* Bright Source Catalog (Voges et al. 1999) have the corresponding fields blank. One new addition to the list of probable members, TYC 3313-1551-1, stands out as by far the most powerful X-ray source at $L_X = 1.5 \times 10^{31}$, exceeding the empirical saturation limit of $\log L_X/L_{bol} \approx -3$. The star is not known to be binary, and it passes all the kinematic and photometric tests as a bona fide member. The nature of this extraordinary activity deserves further investigation.

Distributions of absolute magnitudes, distances from the cluster's center, deviations from the streaming motion Δ/σ_Δ, and tangential velocities perpendicular to the streaming motion $v_\perp$ (§ 4) are depicted in Figure 7 separately for stars confidently detected as X-ray emitters and those studied but not detected. The samples are sadly small, but significant conclusions can be drawn. Stars earlier than G are usually weak X-ray sources, which is a well-established and theoretically justified fact. The second column of plots in Figure 7 suggests that the prominent emitters are less concentrated around the center, and many of them are spread far beyond the tidal radius, which is likely less than 10 pc. The most handy explanation to this could be a mass segregation that gathers the massive, nonemitting stars in the core. However, there is no evidence of a virialized state for α Persei (§ 10). It appears that the extended halo around the cluster, whose origin is an open issue, is intrinsically rich in active rotators. The remaining two columns of plots pertain to the observed dispersion of velocities per coordinate relative to the common streaming motion. We have seen (§ 4) that the astrometric data suggest a low dispersion much smaller than 1.1 km s^{-1}. Separated in two groups, we find again well-confined, quasi-Gaussian distributions indistinguishable between the X-ray emitters and weak emitters, consistent with zero physical dispersion. This differentiates α Persei from the Hyades and the Pleiades, where markedly lower internal dispersions are found for strong X-ray emitters (Makarov 2000; Makarov & Robichon 2001). The latter two clusters are closer to the Sun and have more identified members, resulting in higher accuracy of kinematic parameters. To sum up, within the available astrometric precision, stars in α Persei appear to have zero dispersion of velocities irrespective of their X-radiation strength.

9. STARS EJECTED FROM α PERSEI

On theoretical grounds, open clusters are deemed short-lived structures, most of which are bound to disperse in just a few hundred megayears. Internal dynamical interactions between member stars, in which hard massive binaries take an especially active role, and chance encounters with gas and molecular clouds result in a steady loss of stars from a gravitationally bound system. The most profuse ejection takes place during the relatively short initial span of a cluster's lifetime, when most of the primordial gas has been swept out by the first massive stars. The rapid loss of mass makes the cluster kinetically overheated. The dynamic ejection, because of the Galactic tidal force, is not isotropic. Stars moving out along the Galactic center direction or in the opposite direction have better chances to escape the cluster than those thrown out at the same velocity in other directions. The latter can wander around for a long time, approaching the parent cluster or its remnant periodically in an epicyclic fashion. Such gravitationally unbound but loosely coherent remnants may account for the fairly old comoving swarms of stars, e.g., the Ursa Major group.

Although theoretically well-studied and discussed, the dynamical ejection of stars from mature, dynamically settled clusters has not obtained much observational evidence. Hoogerverf et al. (2001) make a bold attempt to find the hosts of the nearest runaway stars, presumably thrown out of binary systems by a supernova explosion of the more massive companion. Their analysis suffers from the large uncertainties in the radial velocities and parallaxes of these distant, hot stars. Compared to these rare phenomena, ejection of ordinary dwarfs from nearby Galactic clusters should be common. Detection of nearby field stars ejected in

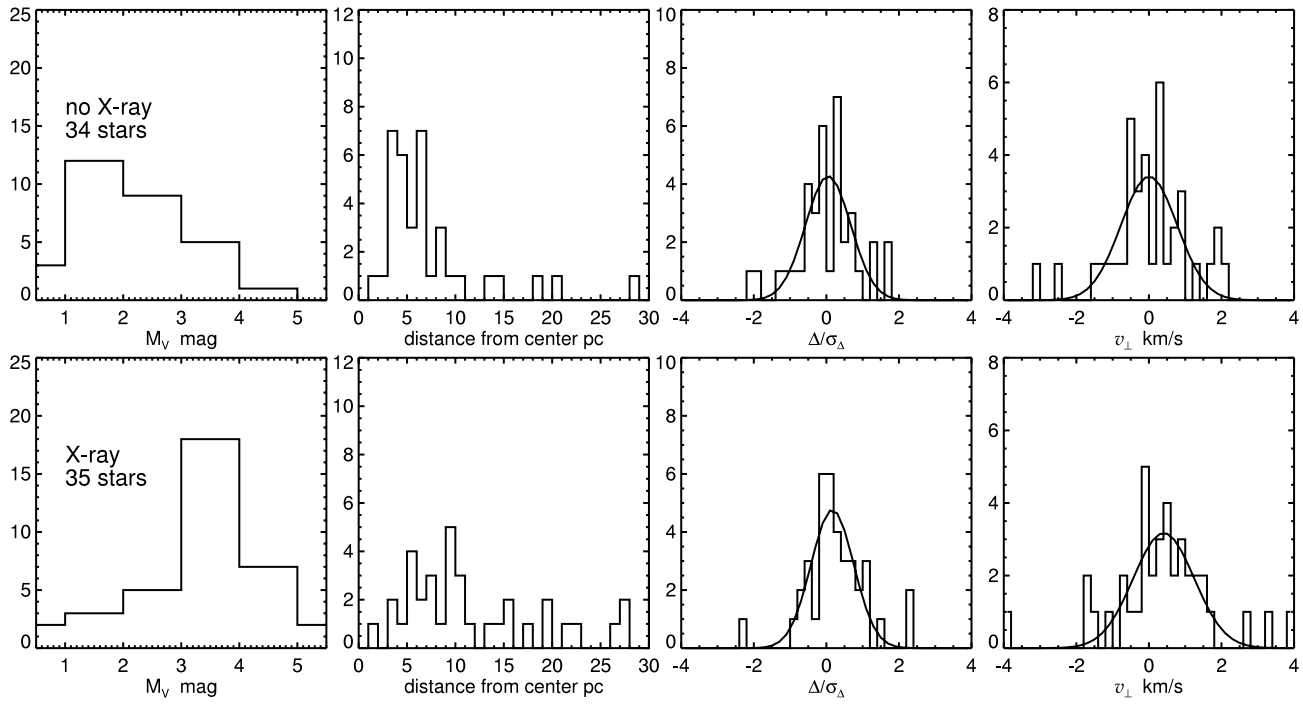

FIG. 7.—Distributions of absolute V magnitudes, distances from the cluster's center, and transverse tangential velocities for stars emitting X-rays and stars without detectable X-radiation. Gaussian fits are shown where appropriate.

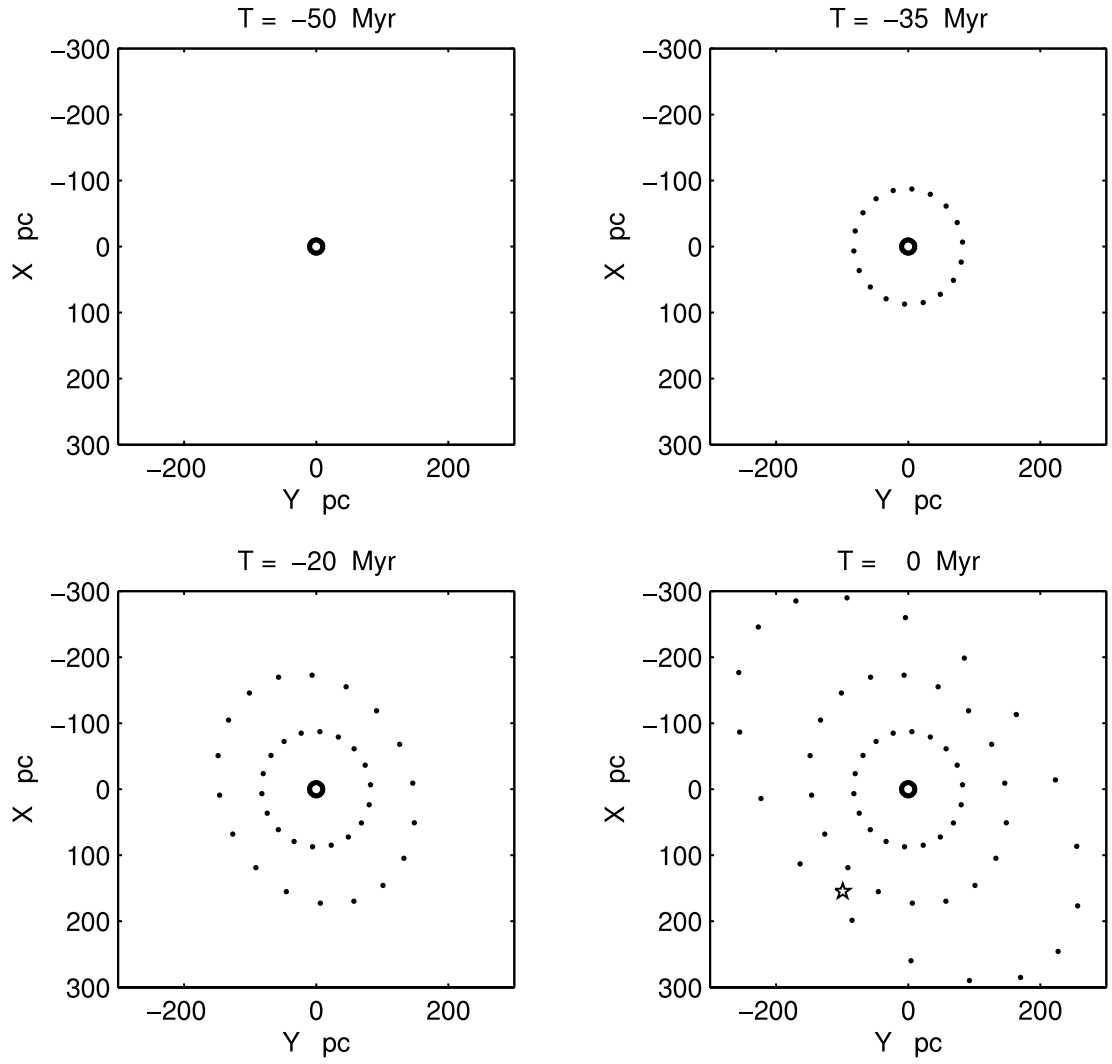

FIG. 8.—Positions of stars isotropically ejected from α Persei at 5 km s^{-1} in the Galactic plane at -50, -35, and -20 Myr and the present. The location of the Sun is shown with a star.

the past from α Persei is of special interest, because such stars can be dated to excellent accuracy. This will facilitate investigations of planet formation in open clusters, the origin of Vega-like stars, and the chromospheric activity of late-type stars. Eventually, all nearby field stars younger than the Pleiades can be traced back to their places of origin.

Using the accurately determined heliocentric space velocity of α Persei, $(U, V, W) = (-15.0, -25.3, -7.6)$ km s^{-1}, I undertake a search of stars whose orbits crossed the cluster in the past 60 Myr using the linear epicycle formalism in Makarov et al. (2004). This linear approximation of the Galactic force is sufficiently accurate for stars that have velocities not too different from the motion of the LSR (as most nearby field stars do). The Geneva-Copenhagen spectroscopic survey of *Hipparcos* F, G, and K stars supplied radial velocities for more than 14,000 stars with trigonometric parallaxes and Tycho-2 proper motions (Nordström et al. 2004). A number of nearby M dwarfs with signs of X-ray or other activity are added to this set of solar-type stars. Each star is tracked back in time for 70 Myr at a 0.25 Myr grid, and its past positions are compared with those of the cluster. To further reduce the number of chance intersections, only stars with accurately measured radial velocities and only encounters prior to 10 Myr ago are considered. The upper limit on the closest distance is set at 15 pc. Unfortunately, the limited precision of the astrometric data does not allow the use of more stringent criteria for the closest approach. A typical error in the initial relative velocity of 0.5 km s^{-1} from the formal errors of the proper motions runs up to $\approx$5 pc positional uncertainty in just 10 Myr. Thus, a great deal of real ejecta are expected to be washed out by the astrometric errors in this analysis, and unrelated field stars to accidentally meet the criteria. Additional signs of stellar youth need to be found to identify the most probable candidates.

Somewhat surprisingly, among the tested 9300 stars meeting these criteria, I find only one plausible ejection event. The nearby M dwarf GJ 82 = HIP 9291 was likely ejected from the α Persei cluster 47 Myr ago at a relative velocity of 5.1 km s^{-1}. The minimum distance from the center of gravity at this time is estimated at 5 pc, with a large uncertainty because of the input data errors and imprecision of the Galactic potential model. This star is one of the relatively few M dwarfs in the Gliese catalog with a strong emission in Hα of 4.73 in equivalent width (Stauffer & Hartmann 1986). Youth is considered the principal reason for such unusual (among the field stars) chromospheric activity in M dwarfs, probably conditioned by a higher rate of rotation. At the same time, this level of emission is quite common among the members of α Persei; in fact, GJ 82 at $V - I = 2.76$ lies at the lower end of the observed spread of Hα equivalent widths for stars of similar mass (Prosser & Randich 1998, see their Fig. 2). Figure 8 shows that a star ejected from α Persei at 5 km s^{-1} could in fact reach the immediate solar neighborhood today, owing mostly to the fact that the Sun has been approaching the cluster for most of the past 50 Myr.

10. DISCUSSION

Is α Persei a cluster? The marked sparsity of the system, the huge halo populated with fairly massive stars, and the proximity to the Cas-Tau association prompted researchers to call it a moving group in earlier literature. However, the tidal radius of a gravitationally bound cluster in the local part of the Galaxy is approximately

$$r_t = 1.4M^{1/3}, \quad (6)$$

where M is the total mass in $M_\odot$. From this, the critical density that makes a system of stars be gravitationally bound (a cluster) is 0.66 $M_\odot$ pc^{-3}. If a total of 100 $M_\odot$ is confined to a sphere of radius 6.5 pc, the system qualifies as a cluster. Using the kinematic parallaxes for individual stars, we find that about 30 stars and binary systems from Table 1 are within this radius.[1] It is recalled that each of these stars is more massive than the Sun, and yet their total mass is likely less than 100 $M_\odot$. A significant number of stars with $M_V > 5$, missing in the sample drawn from Tycho-2, are expected to lie in the central region, contributing the required bounding mass. It should be noted that the number of true members with masses below the solar mass remains quite uncertain. Prosser (1992) obtains a remarkably flat luminosity function for M_V between 4 and 11 mag (with a dip at 8) and interprets this feature as incompleteness of his survey. Our Figure 5 reveals a large contamination by nonmembers abruptly starting at $(J - K_s) = 0.2$ and a curiously uniform distribution of possible members between 0.2 and 0.5. Unlike the Pleiades, whose mass function scales as $M^{-1.05}$ down to approximately 0.2 $M_\odot$ (Adams et al. 2001), the contribution of the lower mass stars in the total mass may be rather modest. On the other hand, also counting field stars that contribute roughly one-sixth of the critical density, it should be sufficient to reach the bound state.

Kroupa et al. (2001) offer a formation scenario of a Pleiades-like cluster, substantiated by detailed *N*-body simulations, from a star-forming core resembling the Orion nebula cluster. This core is characterized by a large number of protostars (10^4) confined to a small area of approximately 0.3–0.5 pc radius. It is predicted that such clusters lose two-thirds of the original members after the natal gas expulsion. Depending on the initial parameters, different models predict one-dimensional velocity dispersions in the range from 0.5 to 1.0 km s^{-1} long after the relaxation time. The tidal radius is expected to decrease slowly due to the continuous mass loss, whereas the percentile radii increase gradually with time between 10 and 100 Myr. In view of the vanishingly small velocity dispersion, mild contraction seen from the discrepancy of the astrometric and spectroscopic radial velocities, and the low number density of members in the core, this scenario does not fit the properties of α Persei. The formation site of α Persei was fundamentally different from the Orion cluster. The basic parameter that seems to determine the dynamical evolution of young clusters is the initial number density. The Orion star-forming region (SFR) is a dense, relatively small area in which newborn stars have (presumably) large velocities up to several km s^{-1}. The crossing time is short, the relaxation time is short, and the dynamical interaction of stars plays a major role under such circumstances. Remaining members are ejected occasionally by encounters with massive binaries, which soon settle in the central region (mass segregation). This is not what we find for α Persei. It is likely that the cluster was formed with a large initial size and small density of stars. The relaxation time is proportional to $R_{\rm core}^{3/2}$ (Chandrasekhar 1942), and for large initial radii and moderate masses can be up to $\approx$100 Myr. The simulations by Lada et al. (1984), in which the stars are formed nonvirialized with almost zero velocity with respect to the center of mass, are more pertinent to this case. The stars that originally had significant velocities escaped the SFR and formed the extended halo at approximately the same time as the gas was expelled by the first massive stars. Stars with nearly zero velocity remained inside the tidal radius and began to be involved in a slow collapse. The crossing time is longer than the cluster's age, and dynamical interaction between members is quite rare. The low initial density may account for the small fraction of

[1] Note that the estimated distances from the cluster's center are imprecise, so that a larger number of members are probably closer than 6.5 pc.

binaries, the lack of short-period binaries, and the small mass ratios in the known spectroscopic binaries. In α Persei, we may be seeing the result of a process essentially different from the Orion-type star formation.

The research described in this paper was carried out at the Jet Propulsion Laboratory, California Institute of Technology, under a contract with the National Aeronautics and Space Administration. This research has made use of the SIMBAD database, operated at CDS, Strasbourg, France, and data products from 2MASS, which is a joint project of the University of Massachusetts and the Infrared Processing and Analysis Center, California Technology Institute, funded by NASA and the NSF. The author is grateful to the referee, D. Soderblom, for helpful comments.

REFERENCES

Adams, J. D., Stauffer, J. R., Monet, D. G., Skrutskie, M. F., & Beichman, C. A. 2001, AJ, 121, 2053
Artyukhina, N. M. 1972, Astron. Zh., 49, 389
Bonatto, Ch., Bica, E., & Girardi, L. 2004, A&A, 415, 571
Carpenter, J. M. 2001, AJ, 121, 2851
Chandrasekhar, S. 1942, Principles of Stellar Dynamics (Chicago: Univ. Chicago Press)
de Zeeuw, P. T., Hoogerwerf, R., de Bruijne, J. H. J., Brown, A. G. A., & Blaauw, A. 1999, AJ, 117, 354
Eddington, A. S. 1910, MNRAS, 71, 43
Eggen, O. J. 1983, MNRAS, 204, 391
Fabricius, C., et al. 2002, A&A, 384, 180
Gunn, J. E., Griffin, R. F., Griffin, R. E. M., & Zimmerman, B. A. 1988, AJ, 96, 198
Heckmann, V. O., Dieckvoss, W., & Kox, H. 1956, Astron. Nachr., 283, 109
Høg, E., et al. 2000a, A&A, 355, L27
———. 2000b, A&A, 357, 367
Hoogerverf, R., de Bruijne, J. H. J., & de Zeeuw, P. T. 2001, A&A, 365, 49
Kroupa, P. 1995, MNRAS, 277, 1522
Kroupa, P., Aarseth, S., & Hurley, J. 2001, MNRAS, 321, 699
Lada, C. J., Margulis, M., & Dearborn, D. 1984, ApJ, 285, 141
Littlefair, S. P., et al. 2003, MNRAS, 345, 1205
Madsen, S., Dravins, D., & Lindegren, L. 2002, A&A, 381, 446
Madsen, S., Dravins, D., Ludwig, H.-G., & Lindegren, L. 2003, A&A, 411, 581
Maíz-Apellániz, J. 2005, PASP, 117, 615
Makarov, V. V. 2000, A&A, 358, L63
Makarov, V. V., & Kaplan, G. H. 2005, AJ, 129, 2420
Makarov, V. V., Odenkirchen, M., & Urban, S. 2000, A&A, 358, 923
Makarov, V. V., Olling, R. P., & Teuben, P. J. 2004, MNRAS, 352, 1199
Makarov, V. V., & Robichon, N. 2001, A&A, 368, 873
Meynet, G., Mermilliod, J.-C., & Maeder, A. 1993, A&AS, 98, 477
Montes, D., et al. 2001, A&A, 379, 976
Morrell, N., & Abt, H. 1992, ApJ, 393, 666
Nordström, Å., et al. 2004, A&A, 418, 989
Patience, M. H., Ghez, A. M., Reid, I. N., & Matthews, K. 2002, AJ, 123, 1570
Perryman, M. A. C., et al. 1997, The *Hipparcos* and Tycho Catalogues (ESA SP-1200; Noordwijk: ESA)
Pietrinferni, A., Cassisi, S., Salaris, M., & Castelli, F. 2004, ApJ, 612, 168
Pinsonneault, M. H., Stauffer, J., Soderblom, D. R., King, J. R., & Hanson, R. B. 1998, ApJ, 504, 170
Press, W. H., Teukolsky, S. A., Vettering, W. T., & Flannery, B. P. 1992, Numerical Recipes in FORTRAN (Cambridge: Cambridge Univ. Press)
Prosser, C. F. 1992, AJ, 103, 488
Prosser, C. F., & Randich, S. 1998, Astron. Nachr., 319, 201
Prosser, C. F., Randich, S., & Simon, T. 1998, Astron. Nachr., 319, 215
Prosser, C. F., Randich, S., Stauffer, J. R., Schmitt, J. H. M. M., & Simon, T. 1996, AJ, 112, 1570
Raboud, D., & Mermilliod, J.-C. 1998, A&A, 329, 101
Randich, S., Schmitt, J. H. M. M., Prosser, C. F., & Stauffer, J. R. 1996, A&A, 305, 785
Robichon, N., Arenou, F., Mermilliod, J.-C., & Turon, C. 1999, A&A, 345, 471 (RAMT)
Shatsova, R. B. 1981, Soviet Astron. Lett., 7, 398
Stauffer, J. R., Caillault, J.-P., Gagné, M., Prosser, C. F., & Hartmann, L. W. 1994, ApJS, 91, 625
Stauffer, J. R., & Hartmann, L. W. 1986, ApJS, 61, 531
Stauffer, J. R., Hartmann, L. W., Burnham, J. N., & Jones, B. F. 1985, ApJ, 289, 247
Stauffer, J. R., Hartmann, L. W., & Jones, B. F. 1989, ApJ, 346, 160
Stauffer, J. R., et al. 2003, AJ, 126, 833
Stern, R. A., Schmitt, J. H. M. M., & Kahabka, P. T. 1995, ApJ, 448, 683
Voges, W., et al. 1999, A&A, 349, 389
Zacharias, N., et al. 2004, AJ, 127, 3043